

# The Magnetic Field of the Large Magellanic Cloud Revealed Through Faraday Rotation

B. M. Gaensler,<sup>1,2\*</sup>, M. Haverkorn,<sup>1</sup> L. Staveley-Smith,<sup>3</sup> J. M. Dickey,<sup>4</sup>  
N. M. McClure-Griffiths,<sup>3</sup> J. R. Dickel,<sup>5</sup> and M. Wolleben<sup>6</sup>

<sup>1</sup>Harvard-Smithsonian Center for Astrophysics, 60 Garden Street MS-6, Cambridge, MA 02138, USA

<sup>2</sup>School of Physics, University of Sydney, NSW 2006, Australia

<sup>3</sup>Australia Telescope National Facility, CSIRO, PO Box 76, Epping, NSW 1710, Australia

<sup>4</sup>Physics Department, University of Tasmania, GPO Box 252-21, Hobart, Tasmania 7001, Australia

<sup>5</sup>Astronomy Department, University of Illinois, 1002 West Green Street, Urbana, IL 61801, USA

<sup>6</sup>Max-Planck-Institut für Radioastronomie, Auf dem Hügel 69, D-53121 Bonn, Germany

\*To whom correspondence should be addressed; E-mail: bgaensler@cfa.harvard.edu

**We have measured the Faraday rotation toward a large sample of polarized radio sources behind the Large Magellanic Cloud (LMC), to determine the structure of this galaxy's magnetic field. The magnetic field of the LMC consists of a coherent axisymmetric spiral of field strength  $\sim 1$  microgauss. Strong fluctuations in the magnetic field are also seen, on small ( $< 0.5$  parsecs) and large ( $\sim 100$  parsecs) scales. The significant bursts of recent star formation and supernova activity in the LMC argue against standard dynamo theory, adding to the growing evidence for rapid field amplification in galaxies.**

The Milky Way and many other spiral galaxies show well-organized, large-scale magnetic fields (1, 2, 3), the existence of which points to a powerful and ubiquitous process which organizes random motions into coherent magnetized structures. The underlying mechanism is believed to be a dynamo, in which magnetic fields are slowly ordered and amplified due to the

interplay between turbulence and differential rotation (4, 5). Magnetism in galaxies is usually mapped by observing the orientation of polarized optical and radio emission from the galaxy itself (3), but these data have limited spatial resolution (6) and can be difficult to interpret (7). An alternative, direct determination of the geometry and strength of magnetic fields comes from the Faraday rotation of background radio sources (8, 9, 10), an effect in which birefringence in an intervening magneto-ionized source rotates the plane of linearly polarized radiation. Measurements of background rotation measures (RMs) are free from the difficulties associated with studying polarized emission produced by the source itself, which suffer from a complicated combination of internal and external Faraday rotation, depolarization, and optical extinction.

We have studied the magnetic field of the LMC, using 1.4-GHz polarization data recorded as part of a hydrogen line survey (11) carried out with the Australia Telescope Compact Array (12). Over a field of 130 square degrees, we have calculated RMs for 291 polarized background sources. Of this sample, about 100 sources lie directly behind the LMC. We used 140 measurements of sources lying outside the LMC to subtract a mean RM, presumably resulting from foreground Faraday rotation in the Milky Way. The resulting distribution of residual Faraday rotation (Fig. 1) shows a strong excess in RM across the extent of the LMC. The implied magnetic field demonstrates spatial coherence: the eastern half of the galaxy shows predominantly positive RMs, while in the west the RMs are mainly negative.

We have converted position on the sky to a location within the LMC disk for each RM measurement, assuming that the galaxy is inclined to the plane of the sky at an angle  $i = 35^\circ$ , with its line of nodes at a position angle  $\Theta = 123^\circ$  (measured north through east) (13). The resulting dependence of RM against position angle within the disk of the LMC (Fig. 2) shows a systematic variation, with the maximum mean RM occurring near the line of nodes. These data can be well fit by a sinusoid of amplitude  $RM_0 = 53 \pm 3 \text{ rad m}^{-2}$ , demonstrating that the coherent component of the LMC's magnetic field has an axisymmetric spiral geometry (14), as

is seen in other galaxies (2, 3, 14). The phase of this cosinusoid corresponds to the pitch angle,  $p$ , of the spiral field (14), but in this case we can only infer a weak constraint,  $|p| \lesssim 20^\circ$ , especially given that the uncertainty on  $\Theta$  is  $\gtrsim 10^\circ$  (13).

In addition to the coherent field, a structure function analysis indicates random fluctuations in RM, with a standard deviation  $\Sigma_{\text{RM}} = 81 \text{ rad m}^{-2}$ , and occurring on a characteristic angular scale of  $\approx 0.1^\circ$ , or  $L \approx 90$  parsecs at the distance to the LMC of 50 kpc. This may represent the evolved supernova remnants (SNRs) and wind bubbles whose interlocking shells dominate the morphology of ionized gas in the LMC on this scale (15).

To estimate the relative strength of the ordered and random field components, we assumed that ionized gas in the LMC consists of a disk of projected thickness  $D$ , in which cells of linear size  $L$  contain clumps of ionized gas of filling factor  $f$  and density  $n_e$  (16). In each cell the magnetic field is comprised of a uniform component of strength  $B_0$  plus a randomly oriented component of strength  $B_R$ . If  $B_R$  is uncorrelated with fluctuations in  $n_e$ , it can be shown that:

$$\frac{\Sigma_{\text{RM}}}{|\text{RM}_0|} \approx \left[ \frac{L}{2fD} \left( 1 + \frac{2}{3} \frac{B_R^2}{B_0^2 \sin^2 i} \right) \right]^{1/2} \quad (1)$$

The occupation length,  $fD$ , of ionized gas is  $\text{DM}_0^2/\text{EM}_0 \approx 530 \text{ pc}$ , where  $\text{DM}_0 \equiv \int n_e dl \approx 100 \text{ cm}^{-3} \text{ pc}$  and  $\text{EM}_0 \equiv \int n_e^2 dl \approx 19 \text{ pc cm}^{-6}$  are the average dispersion measure (DM) and median extinction-corrected emission measure (EM) integrated through the LMC, respectively (12). Equation (1) then implies  $B_R/B_0 = 3.6$ : the random field dominates the ordered field, as seen in many other galaxies (2, 17).

The actual values of  $B_0$  and  $B_R$  can also be estimated. If  $B_R$  and fluctuations in  $n_e$  are uncorrelated, then the strength of the ordered component of the LMC's magnetic field is

$$B_0 = \frac{|\text{RM}_0|}{K \text{DM}_0 \sin i} \approx 1.1 \mu\text{G}, \quad (2)$$

where  $K = 0.81 \text{ rad m}^{-2} \text{ pc}^{-1} \text{ cm}^3 \mu\text{G}^{-1}$ . The strength of the random field is then  $B_R = 3.6B_0 \approx 4.1 \mu\text{G}$ , and the total magnetic field strength on large scales is  $B_T = (B_0^2 + B_R^2)^{1/2} \approx$

4.3  $\mu\text{G}$ . We note that in selected regions where  $B$  and  $n_e$  are correlated, as might result from compression in SNR shocks, the above approach overestimates  $B_0$  and underestimates  $B_R$ , each by factors of  $\sim 2$  (17).

The polarized background sources are not randomly distributed across the LMC’s extent, but tend to avoid areas of bright  $\text{H}\alpha$  emission (Fig. 1). Specifically, background sources are increasingly depolarized as they propagate through regions of higher EM (Fig. 3). This suggests that we are observing beam depolarization, in which small-scale fluctuations in foreground RM produce interference between polarized rays along adjacent sightlines (7). Beam depolarization is only significant when the angular scale of RM fluctuations is smaller than the resolution of the data and the scale of intrinsic polarized structures. While the resolution here,  $\sim 40$  arcsec, is comparatively large, extragalactic sources are typically of much smaller angular extent: for 1.4-GHz flux densities in the range 10–300 millijanskys as observed here, the median angular size is only  $\approx 6$  arcsec (18), or  $\approx 1.5$  parsecs when projected against the LMC. The depolarization (Fig. 3) implies strong RM fluctuations on scales  $l \ll 1.5$  parsecs. In such a situation, beam depolarization reduces the intrinsic linearly polarized intensity,  $P_0$ , to a level (19, 7):

$$P = P_0 e^{-2\sigma_{\text{RM}}^2 \lambda^4}, \quad (3)$$

where  $\lambda$  is the observing wavelength and  $\sigma_{\text{RM}}$  is the standard deviation in RMs across the source. To account for the dependence of  $P/P_0$  on EM (Fig. 3), we need to relate  $\sigma_{\text{RM}}$  to the EM along a given sightline. If the magnetic field is uncorrelated with the ionized gas density, we expect that  $\sigma_{\text{RM}} = k \text{ EM}^{1/2}$ , where  $k$  is a constant. With this assumption, the fluctuating magnetic field on a scale  $l$  parsecs needed to produce the observed depolarization has a strength  $B_r \approx k(lK^2/3)^{-1/2} \mu\text{G}$ . In Figure 3, Equation (3) has been fit to the data for  $P_0 \approx 0.104$  and  $k \approx 1.8 \text{ rad m}^{-2} \text{ pc}^{-1/2} \text{ cm}^3$ . Assuming  $l < 0.5$  parsecs, we find that  $B_r > 5 \mu\text{G}$ . We thus infer that there are significant RM and magnetic field fluctuations on sub-parcsec scales in the

ionized gas of the LMC. This phenomenon is also seen in our own Galaxy, and may trace the turbulent winds and H II regions of individual stars (20, 21).

Most spiral galaxies are long-lived systems that exhibit significant rotational shear and that experience relatively constant star-formation rates over long periods of time. Coherent magnetic fields in these galaxies are believed to be produced by a dynamo mechanism, in which small-scale turbulent magnetic fields are amplified and ordered by cyclonic motions and differential rotation (2, 4, 5). However, in galaxies dominated by sudden bursts of star formation and supernova activity, the dramatic injection of energy should disrupt the slow monotonic increase of the large-scale field produced by a standard turbulent dynamo (22, 23). The LMC has experienced several intense bursts of star formation over the past  $\sim 4$  Gyr triggered by repeated close encounters with the Milky Way and with the Small Magellanic Cloud (24, 25), and yet still maintains a coherent spiral magnetic field. Combined with previous results demonstrating the presence of ordered magnetic fields in young galaxies for which the dynamo has had little time to operate (26), and in irregular galaxies which lack significant amounts of rotation (27), there is now evidence that standard dynamo processes are ineffective in the LMC and these other galaxies. There are several viable alternatives to explain the coherent magnetic fields that we observe. Potentially most pertinent for the LMC is the cosmic-ray driven dynamo, in which recent supernova activity generates a significant population of relativistic particles. The buoyancy of these particles inflates magnetic loops out of the disk; adjacent loops reconnect, and then are amplified by differential rotation to generate a large-scale spiral field (28, 29). This mechanism not only requires vigorous star formation, as has occurred recently for the LMC, but has a time scale for amplification of only  $\sim 0.2$  Gyr (29), and so can quickly generate large-scale magnetic fields before they are dissipated by outflows and tidal interactions. This process can thus potentially account for the coherent fields seen in the LMC and other galaxies (30).

## References and Notes

1. R. Beck, A. Brandenburg, D. Moss, A. Shukurov, D. Sokoloff, *ARA&A* **34**, 155 (1996).
2. R. Beck, *Philos. Trans. Roy. Soc. London A* **358**, 777 (2000).
3. J.-L. Han, R. Wielebinski, *Chin. J. Astron. Astrophys.* **2**, 293 (2002).
4. A. A. Ruzmaikin, D. D. Sokolov, A. M. Shukurov, *Magnetic Fields of Galaxies* (Kluwer, Dordrecht, 1988).
5. R. M. Kulsrud, *ARA&A* **37**, 37 (1999).
6. A. Fletcher, E. M. Berkhuijsen, R. Beck, A. Shukurov, *A&A* **414**, 53 (2004).
7. D. D. Sokoloff, *et al.*, *MNRAS* **299**, 189 (1998).
8. J. C. Brown, A. R. Taylor, B. J. Jackel, *ApJS* **145**, 213 (2003).
9. J. L. Han, R. Beck, E. M. Berkhuijsen, *A&A* **335**, 1117 (1998).
10. B. M. Gaensler, R. Beck, L. Feretti, *New Astronomy Reviews* **48**, 1003 (2004).
11. S. Kim, *et al.*, *ApJ* **503**, 674 (1998).
12. Materials and methods are available as supporting material on Science Online.
13. R. P. van der Marel, *The Local Group as an Astrophysical Laboratory*, M. Livio, ed. (Cambridge University Press, Cambridge, 2004). In press (astro-ph/0404192).
14. M. Krause, E. Hummel, R. Beck, *A&A* **217**, 4 (1989).
15. J. Meaburn, *MNRAS* **192**, 365 (1980).

16. The depolarization demonstrated in Figure 3 implies that the observed RMs do not probe ionized gas in bright individual H II regions, making this a reasonable assumption.

17. R. Beck, A. Shukurov, D. Sokoloff, R. Wielebinski, *A&A* **411**, 99 (2003).

18. R. A. Windhorst, E. B. Fomalont, R. B. Partridge, J. D. Lowenthal, *ApJ* **405**, 498 (1993).

19. B. J. Burn, *MNRAS* **133**, 67 (1966).

20. J. P. Leahy, *MNRAS* **226**, 433 (1987).

21. M. Haverkorn, B. M. Gaensler, N. M. McClure-Griffiths, J. M. Dickey, A. J. Green, *ApJ* **609**, 776 (2004).

22. P. P. Kronberg, *Rep. Prog. Phys.* **57**, 325 (1994).

23. K. T. Chyzy, R. Beck, *A&A* **417**, 541 (2004).

24. E. W. Olszewski, N. B. Suntzeff, M. Mateo, *Ann. Rev. Astr. Ap.* **34**, 511 (1996).

25. K. Bekki, M. Chiba, *MNRAS* **356**, 680 (2005).

26. P. P. Kronberg, J. J. Perry, E. L. H. Zukowski, *ApJ* **387**, 528 (1992).

27. K. T. Chyzy, R. Beck, S. Kohle, U. Klein, M. Urbanik, *A&A* **355**, 128 (2000).

28. D. Moss, A. Shukurov, D. Sokoloff, *A&A* **343**, 120 (1999).

29. M. Hanasz, G. Kowal, K. Otmianowska-Mazur, H. Lesch, *ApJ* **605**, L33 (2004).

30. K. Otmianowska-Mazur, K. T. Chyzy, M. Soida, S. von Linden, *A&A* **359**, 29 (2000).

31. J. E. Gaustad, P. R. McCullough, W. Rosing, D. Van Buren, *PASP* **113**, 1326 (2001).

32. We are grateful to Sungeun Kim for carrying out the original ATCA observations which made this project possible. We also thank Rainer Beck, Richard Crutcher, Katarzyna Otmianowska-Mazur, Detlef Elstner and Dmitry Sokoloff for useful discussions. The Southern H-Alpha Sky Survey Atlas (SHASSA) is supported by the National Science Foundation. The Australia Telescope is funded by the Commonwealth of Australia for operation as a National Facility managed by CSIRO. B.M.G. acknowledges the support of the National Science Foundation through grant AST-0307358, and of the University of Sydney through the Denison Fund.

### **Supporting Online Material**

[www.sciencemag.org](http://www.sciencemag.org)

Materials and Methods

## FIGURE CAPTIONS

**FIGURE 1:** Faraday rotation measures through the Large Magellanic Cloud. The image shows the distribution of emission measure toward the LMC in units of  $\text{pc cm}^{-6}$ , derived from the Southern H-Alpha Sky Survey Atlas (31). The symbols show the position, sign and magnitude of the baseline-subtracted RM measurements (12): filled and open circles (both marked in green) correspond to positive and negative RMs, respectively, while asterisks (marked in purple) indicate RMs which are consistent with zero within their errors. The diameter of each circle is proportional to the magnitude of the RM, the largest positive and negative RMs being  $+247 \pm 13 \text{ rad m}^{-2}$  and  $-215 \pm 32 \text{ rad m}^{-2}$ , respectively.

**FIGURE 2:** RM against position angle within the LMC. The six data points are a binned representation of the 93 RMs which lie within a radius of 3.5 degrees of the center of the EM distribution seen in Fig. 1 (i.e., Right Ascension [J2000]  $05^{\text{h}}16^{\text{m}}03^{\text{s}}$ , Declination [J2000]  $-68^{\circ}41'45''$ ), plotted against deprojected position angle within the LMC, measured from the line of nodes. The uncertainty on each datum is the weighted standard error in the mean for RMs in that bin. The dashed line shows a cosinusoidal least-squares fit to the unbinned data, with an amplitude of  $+53 \pm 3 \text{ rad m}^{-2}$  and an offset from zero of  $+9 \pm 2 \text{ rad m}^{-2}$ . The phase of the cosinusoid is only weakly constrained, falling between  $\pm 15^{\circ}$ . The fit is not a strong function of the center adopted for the LMC.

**FIGURE 3:** Polarized fraction of 81 background sources as a function of EM (12 of the 93 sources shown in Fig. 2 have been excluded: six with  $\text{EM} > 100 \text{ pc cm}^{-6}$ , and six with an observed  $\text{EM} \leq 0 \text{ pc cm}^{-6}$  due to imperfect star subtraction). A Galactic foreground contribution of  $3 \text{ pc cm}^{-6}$  has been subtracted from each EM measurement. The uncertainty for each

binned data-point corresponds to the weighted standard error in the mean for each bin. The observed depolarization as a function of EM cannot be a result of source confusion or other observational selection effects, since sources with RMs were identified from an image of linear polarization, in which the weak signals from diffuse polarized emission show no correlation with  $H\alpha$  emission. It also cannot be due to excessive Faraday rotation across our observing band (bandwidth depolarization), since for the narrow frequency channels (8 MHz) used here, this effect would manifest itself only for  $|RM| > 4000 \text{ rad m}^{-2}$ ,  $\sim 20$  times larger than any RMs observed. The dashed line shows a least-squares fit of Equation (3) to the unbinned data, assuming  $\sigma_{RM} \propto EM^{1/2}$ .

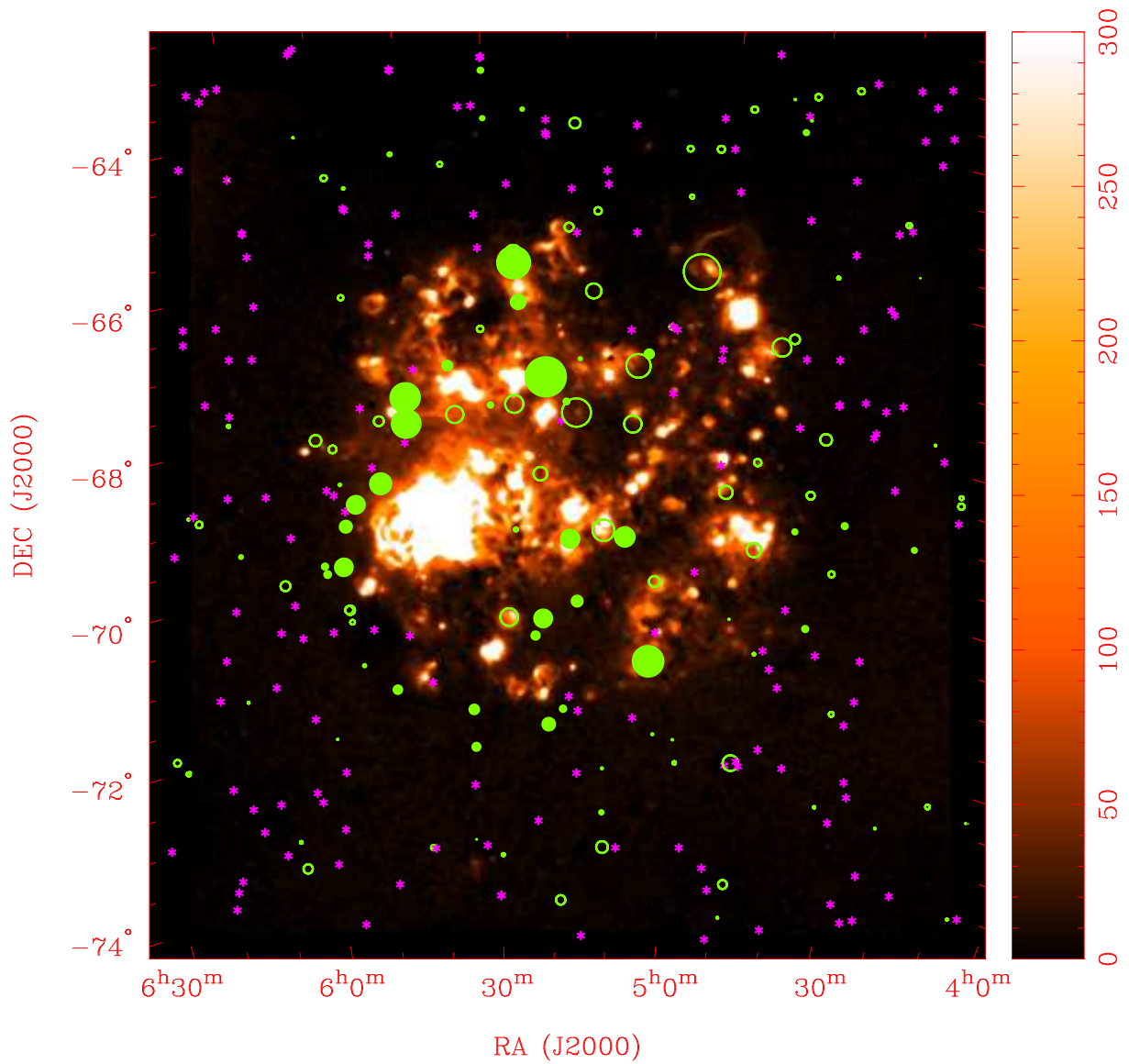


Figure 1:

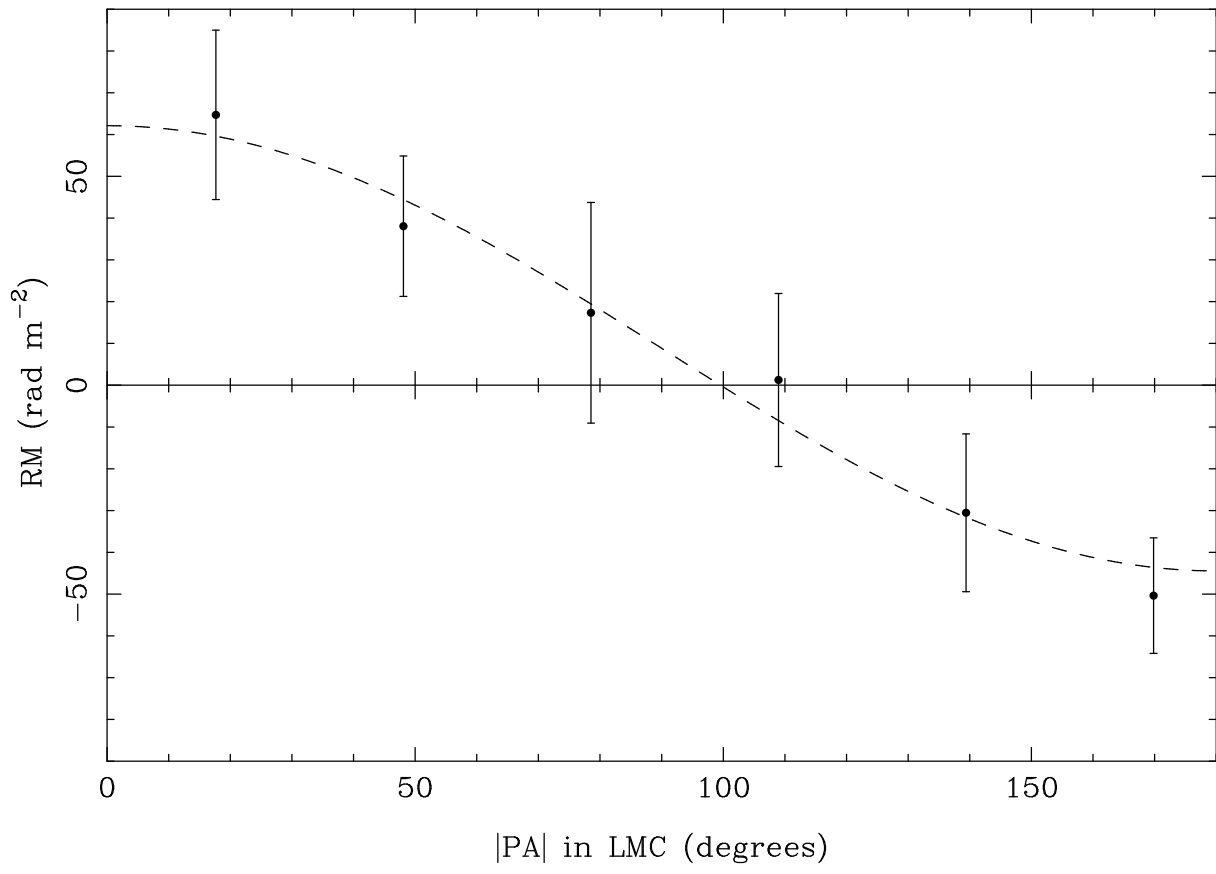


Figure 2:

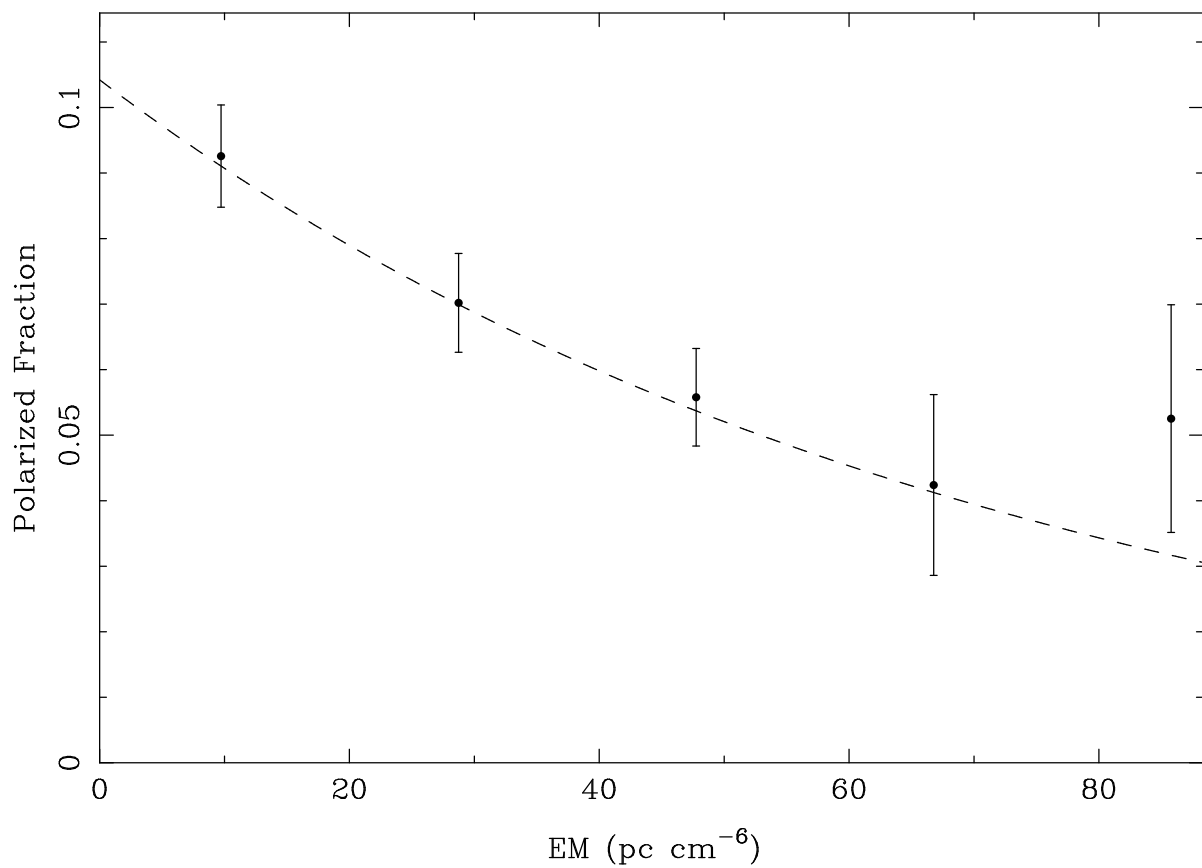


Figure 3:

## SUPPORTING ON-LINE MATERIAL

### Materials and methods

The RMs presented here were determined from a 1.4-GHz mosaic of 1300 pointings toward the LMC, made using the Australia Telescope Compact Array over the period 1994 October to 1996 February at a resolution of 40 arcsec (Kim et al, 1998, *The Astrophysical Journal*, v503, p674). Full polarization was recorded in this survey in 14 successive channels of bandwidth 8 MHz each, with center frequencies between 1328 and 1432 MHz. Antenna gains were calibrated using observations every  $\sim 30$  min of one of PKS B0407–68 or PKS B0454–810, while absolute flux densities and polarization leakages were determined using observations of PKS B1934–638. For each frequency channel, images were formed in Stokes  $Q$  and  $U$  at a pixel size of  $13 \times 13$  arcsec $^2$ , were deconvolved using a maximum entropy algorithm, corrected for primary beam attenuation, and then were combined and debiased to form an image of linear polarization,  $\mathcal{L} = (Q^2 + U^2)^{1/2}$ . Using a false-discovery rate algorithm (Hopkins et al., 2002, *The Astronomical Journal*, v123, p1086) on an average of the 14 images of  $\mathcal{L}$ , 324 polarized sources were identified which were unresolved, did not correspond to a catalogued pulsar or supernova remnant within the LMC, and had a fractional linear polarization between 0.3 and 50 per cent. For each such source, values of Stokes  $Q$  and  $U$  were then extracted from the individual channel maps for nine pixels surrounding the source peak. For each pixel, the RM and its uncertainty were determined from the 14 pairs of  $Q$  and  $U$  values using the algorithm of Brown et al, 2003, *The Astrophysical Journal Supplemental Series*, v145, p213. An individual pixel's RM measurement was accepted only if the pixel had a debiased signal-to-noise in polarization of  $> 1$  in at least eight frequency channels, and if the quality of the RM fit was better than 90%. A source's overall RM was considered valid if at least five of nine pixels had acceptable

RM fits, and if the dispersion in RM between pixels was less than twice the average error in each pixel's RM. Of 324 polarized sources, 291 passed all these tests, with typical errors in RM for each source of  $\pm 20$  rad m $^{-2}$ . By considering 140 RMs at a radius of  $> 4.5$  degrees from the LMC's center, we found that a positive offset in RM was present due to foreground and background contributions; a mean baseline was therefore subtracted from the data in four separate quadrants:  $+33.5 \pm 3.3$  rad m $^{-2}$  in the southeast,  $+22.5 \pm 3.8$  rad m $^{-2}$  in the southwest,  $+49.0 \pm 4.5$  rad m $^{-2}$  in the northwest, and  $+31.3 \pm 3.4$  rad m $^{-2}$  in the northeast.

To estimate the total dispersion measure through the LMC, we used the fact that dispersion of the pulsed signals from the five known radio pulsars in the LMC implies a mean total dispersion measure  $DM \sim 100$  cm $^{-3}$  pc (Crawford et al., 2001, *The Astrophysical Journal*, v553, p367). The foreground contribution to the DM from the Milky Way is  $\approx 50$  cm $^{-3}$  pc (Cordes & Lazio, preprint, <http://arxiv.org/abs/astro-ph/0207156>). If the mean DM of LMC pulsars corresponds to a location half way through the LMC disk, then  $DM_0 \approx 100$  cm $^{-3}$  pc.

Emission measures have been derived from the Southern H-alpha Sky Survey Atlas (Gaus-  
tad et al., 2001, *Publications of the Astronomical Society of the Pacific*, v113, p1326), by cor-  
recting smoothed and star-subtracted H $\alpha$  emission in this region for both foreground extinction  
in the Milky Way and internal extinction in the LMC. In both cases, extinction corrections were  
derived from H I column density maps (Staveley-Smith et al., 2003, *Monthly Notices of the  
Royal Astronomical Society*, v339, p87; Kim et al., 2003, *The Astrophysical Journal Supple-  
mental Series*, v148, 473) using typical gas-to-dust ratios for our Galaxy and for the LMC (Pei,  
1992, *The Astrophysical Journal*, v395, p130), and assuming that extinction within the LMC is  
caused by only half of the LMC H I column. H $\alpha$  intensity was then converted into EM units  
assuming an electron temperature of 8000 K.